Photoreduction of Heme Proteins: Spectroscopic Studies and Cross-Section Measurements

Yuangang Gu, Pusheng Li, J. Timothy Sage, and Paul M. Champion*

Contribution from the Department of Physics, Northeastern University, Boston, Massachusetts 02115

Received November 18, 1992

Abstract: Metmyoglobin, cytochrome *c*, cytochrome b_5, heme octapeptide, and cytochrome P450 are photoreduced without the addition of foreign electron donors, using laser irradiation wavelengths from 430 to 254 nm. Photooxidation is also observed and begins to compete strongly with photoreduction, as the laser excitation is tuned to the UV. These studies demonstrate the universality of photoreduction in heme proteins and suggest that the heme axial ligands play an important, although not exclusive, role in determining the photoreduction cross-section. The photoreduction cross-sections are measured quantitatively as a function of wavelength for the first time, and they show an almost exponential increase as the excitation is tuned into the UV range. This behavior is adequately modelled using near ultraviolet optical transitions with Gaussian line shapes centered near 250 nm. However, an alternative model that considers transient heating of the donor–acceptor vibrational subspace also gives excellent fits to the data. The possibility of transient heating is suggested by the weak temperature dependence of the photoreduction cross-section below 180 K as well as by a significant increase in the cross-section when pulsed laser excitation is used for irradiation. The photoreduced products are characterized by their absorption and resonance Raman spectra and are compared to the chemically reduced species. The distal pocket of myoglobin appears to be slightly modified by photoreduction, but there is no evidence for alteration of cytochrome *c*. The effects of solvent composition and dissolved oxygen on the photoreduction process are also investigated.

I. Introduction

Electron-transfer reactions play a key role in the function of biological systems.[1] For example, in the photosynthetic reaction center, photon excitation and the subsequent charge separation is the ultimate force driving the life process. Although the theory of such reactions in biological systems is still undergoing refinement, the process can generally be considered to involve several steps: the photoexcitation of a donor/acceptor complex, electron transfer, reorganization of the nuclear equilibrium positions, and decay to the thermally equilibrated, charge separated ground state. Extensive experimental work has been focused on the study of electron transfer between fixed metal redox centers in proteins,[2-7] and genetic engineering techniques have been used to make structural modifications in order to test various models for the reaction.[8-12]

On the other hand, several groups have studied the process of photoreduction in native heme proteins and metalloporphyrins by monitoring the absorption spectrum as the sample is irradiated with broad band excitation. Many of the previous studies have utilized external electron donors or sensitizers[13-16] although photoreduction of heme proteins, such as cytochrome *c* and cytochrome P450, has been reported in the absence of foreign donors.[17-21] Resonance Raman (RR) spectroscopy has also been used in studies of heme protein photoreduction, both in solution[22-28] and in single crystals,[29] by measuring the changes in the oxidation marker band, ν_4.

In spite of these efforts, a detailed mechanism for heme photoreduction remains elusive. One of the main puzzles is the identification of the electron donor. Bartocci and co-workers[18] claim that the heme axial ligand provides the electron which is transferred to reduce the heme iron. However, this view is discouraged by the finding[25] that illumination in the iron–ligand

(1) Long-Range Electron Transfer in Biology. In *Structure and Bonding*; Palmer, G., Ed.; Springer-Verlag: Berlin, 1991; Vol. 75.
(2) Nocek, J. M.; Liang, N.; Wallin, S. A.; Mauk, A. G.; Hoffman, B. M. *J. Am. Chem. Soc.* **1990**, *112*, 1623.
(3) Liang, N.; Mauk, A. G.; Pielak, G. J.; Johnson, J. A.; Smith, M.; Hoffman, B. M. *Science* **1988**, *240*, 311.
(4) Natan, M. J.; Hoffman, B. M. *J. Am. Chem. Soc.* **1989**, *111*, 6468.
(5) Bowler, B. E.; Meade, T. J.; Mayo, S. L.; Albin, M.; Gray, H. B. *J. Am. Chem. Soc.* **1989**, *111*, 8757.
(6) Meade, T. J.; Gray, H. B.; Winkler, J. R. *J. Am. Chem. Soc.* **1989**, *111*, 4353.
(7) Gray, H. B.; Malmström, B. G. *Biochemistry* **1989**, *28*, 7499.
(8) Raphael, A. L.; Gray, H. B. *J. Am. Chem. Soc.* **1991**, *113*, 1038.
(9) Concar, D. W.; Whitford, D.; Pielak, G. J.; Williams, R. J. P. *J. Am. Chem. Soc.* **1991**, *113*, 2401.
(10) Everest, A. M.; Wallin, S. A.; Stemp, E. D. A.; Nocek, J. M.; Mauk, A. G.; Hoffman, B. M. *J. Am. Chem. Soc.* **1991**, *113*, 4337.
(11) Liang, N.; Pielak, G. J.; Mauk, A. G.; Smith, M.; Hoffman, B. M. *Proc. Natl. Acad. Sci. U.S.A.* **1987**, *84*, 1249.
(12) Willie, A.; Stayton, P.; Sligar, S.; Durham, B.; Millet, F. *Biochemistry* **1992**, *31*, 7237.
(13) Marinov, B. S. *Photochem. Photobiol.* **1986**, *44*, 665.
(14) Goda, K.; Hisaoka, M.; Ueda, T. *Biochemistry Intnl.* **1987**, *15*, 635.
(15) Gerasimenko, V. V.; Sadovnikova, N. A.; Marinov, B. S. *Studia Biophysica* **1987**, *120*, 123.
(16) Ferri, A.; Patt, D.; Chiozzi, P.; Cattozzo, M.; Bartocci, C.; Maldotti, A. *J. Photochem. Photobiol. B* **1988**, *2*, 341.
(17) Bartocci, C.; Maldotti, A.; Varani, G.; Battioni, P.; Carassiti, V. *Inorg. Chem.* **1991**, *30*, 1255.
(18) Bartocci, C.; Maldotti, A.; Carassiti, V.; Traverso, O. *Inorg. Chimica Acta* **1985**, *107*, 5.
(19) Richman, R. M.; Peterson, M. W. *J. Am. Chem. Soc.* **1985**, *104*, 5795.
(20) Masuda, T.; Minemura, A.; Yamauchi, K.; Kondo, M. *J. Radiat. Res.* **1980**, *21*, 149.
(21) Pierre, J.; Bazin, M.; Debey, P.; Sandus, R. *J. Biochem.* **1982**, *124*, 533.
(22) Adar, F.; Yonetani, T. *Biochim. Biophys. Acta* **1978**, *502*, 80.
(23) Ogura, T.; Yoshikawa, S.; Kitagawa, T. *Biochemistry* **1985**, *24*, 7746.
(24) Kitagawa, T.; Chihara, S.; Fushitani, K.; Morimoto, H. *J. Am. Chem. Soc.* **1984**, *106*, 1860.
(25) Ozaki, Y.; Iriyama, K.; Ogoshi, H.; Kitagawa, T. *J. Am. Chem. Soc.* **1987**, *109*, 5583.
(26) Ogura, T.; Fidler, V.; Ozaki, Y.; Kitagawa, T. *Chem. Phys. Lett.* **1990**, *169*, 457.
(27) Hobbs, J. D.; Wynn, M.; Nunez, D.; Malkin, R.; Knaff, D.; Ondrais, M. *Biochim. Biophys. Acta* **1991**, *1059*, 37.
(28) Verma, A. L.; Chaudhury, N. *J. Raman Spectrosc.* **1991**, *22*, 427.
(29) Sage, J. T.; Morikis, D.; Champion, P. M. *J. Chem. Phys.* **1989**, *90*, 3015.

0002-7863/93/1515-4993$04.00/0

charge-transfer band does not induce the photoreduction. Other groups believe[20,21] that aromatic amino acids, particular tryptophan, are responsible for the electron transfer. Basically, the mechanism of photoreduction in heme proteins, and its wavelength dependence, remains poorly documented.

The work presented here is focused on the photoreduction of heme proteins and heme octapeptide (H8PT) model compounds. Resonance Raman spectra are used to make structural comparisons between photoreduced and chemically reduced samples, and we briefly discuss the role of oxygen and solvent composition in the photoreduction process. We also present the first quantitative measurements of the wavelength dependence of the photoreduction (σ_R) and photooxidation (σ_0) cross-sections for myoglobin, cytochrome *c*, cytochrome b_5, cytochrome P450, and H8PT. These measurements are carried out without adding any foreign electron donors and show an exponential increase of σ_R and σ_0 as the photoreduction wavelength is tuned into the UV range. The photoreduction of cytochrome *c* is demonstrated to be reversible by using multiple wavelengths to sequentially photooxidize and photoreduce the sample.

A simple four-state theoretical model is presented in order to connect the experimentally determined parameters with the fundamental rates governing the electron-transfer process. The exponential wavelength dependence of the cross-sections can be made quantitatively consistent with a model that invokes transient vibrational heating effects or with a more traditional model, which assumes a photoreduction cross-section that scales with an underlying Gaussian absorption band centered near 250 nm. However, measurements of the temperature dependence of the photoreduction rate, along with a significant enhancement of the cross-section using pulsed laser irradiation, suggest that photon driven vibrational heating plays a potentially important role in the transport process.

II. Theory

We consider the photoreduction of heme proteins within a framework of photoexcitation, followed by excited-state electron transfer. We let the system ground state (DA) be excited by photons (with rate k_L^+) to an upper electronic state that can react or decay into a state that is potentially more reactive than the ground state with respect to chemical change of the system (i.e., the excited-state potential surface may be altered so that the free energy favors charge transfer and/or the optically excited DA complex may be vibrationally hot on time scales that are sufficiently long to allow irreversible transitions to product states[30]). We denote the photoexcited, reactive state as $(DA)^*$ with the understanding that it may involve a thermalized photoexcited electronic state, a (vibrationally hot) transiently populated electronic state on the nonradiative decay pathway, or even a vibrationally hot electronic ground state. After the excitation of $(DA)^*$, the system can branch by decaying (k_b^+) to the (thermalized) ground state or by transferring an electron (k_E^+) from donor, D, to acceptor, A, to form an excited state of the reduced system, $(D^+A^-)^*$. This state can either undergo back transfer (k_E^-) or relax (k_b^-) to the charge separated (thermalized) ground state (D^+A^-). Note that the reverse process may also take place (i.e., the reduced system may be photooxidized). However, the oxidized system can be almost totally photoreduced if there exists a higher barrier blocking the electron back transfer in both the ground and excited states. A simple view of the process is sketched in Figure 1.

Figure 1 is a "charge neutral" analysis, since electric charge does not enter or leave the system. An alternative and somewhat more realistic "charge flow" analysis is suggested by photooxidation experiments performed on the chemically reduced species. Such an analysis is briefly discussed in the Appendix. The kinetic

(30) Li, P.; Sage, T.; Champion, P. M. *J. Chem. Phys.* **1992**, *97*, 3214.

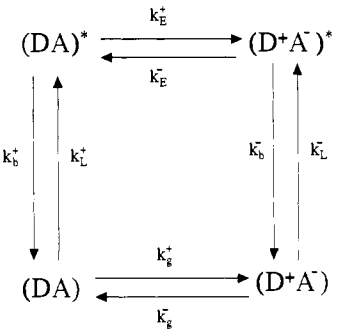

Figure 1. A sketch of a four level system for photoreduction via excited-state population and decay. The *k*'s represent transition rates.

expressions developed in this section hold for either type of analysis. However, it must be kept in mind that when charge flow is allowed different states are in the photoreduction and photooxidation pathways and the interpretation of the fundamental rates is altered (see Appendix).

The kinetics of sequential excited-state electron transfer in a four level system with a time dependent vibrational temperature are potentially quite complicated. To phenomenologically solve this problem, we assume the various rates can be approximated by time independent average quantities, and use the first order rate equation to describe the process

$$\frac{dN_0}{dt} = -(k_L^+ + k_g^+)N_0 + k_b^+N_0^* + k_g^-N_R$$

$$\frac{dN_0^*}{dt} = k_L^+N_0 - (k_b^+ + k_E^+)N_0^* + k_E^-N_R^*$$

$$\frac{dN_R^*}{dt} = k_E^+N_0^* - (k_b^- + k_E^-)N_R^* + k_L^-N_R$$

$$\frac{dN_R}{dt} = k_g^+N_0 + k_b^-N_R^* - (k_L^- + k_g^-)N_R \qquad (1)$$

and

$$1 = N_R + N_R^* + N_0^* + N_0 \qquad (2)$$

where N_0, N_0^*, N_R^*, and N_R are the fractional populations for states (DA), $(DA)^*$, $(D^+A^-)^*$, and (D^+A^-), respectively. The various rates are shown in Figure 1 and it should be understood that

$$k_L^+ = J\sigma_d^+(\nu) \qquad (3)$$

is the rate of photoexcitation into the reactive state $(DA)^*$. Here *J* is the photon flux, and $\sigma_d^+(\nu)$ is the absorption cross-section of a "doorway" transition that leads to the reactive donor–acceptor excited state (note that $\sigma_d^+(\nu)$ is **not** necessarily the absorption cross-section of the heme). The possibility that $(DA)^*$ may not be directly photoexcited is accounted for by including, within $\sigma_d^+(\nu)$, the yield for its production from the directly excited optical state. This approach implicitly assumes that photoexcitation is the rate-limiting step in the creation of $(DA)^*$, so that the nonradiative decay into $(DA)^*$ must be rapid compared to the rate of direct photoexcitation.

The general solution for the four level system is quite complicated, although the steady state solution may easily be obtained ($t \rightarrow \infty$). In some special cases, however, the system may be simplified, and relatively straightforward solutions to eq 1 can be found. In most of the examples studied here, the electron transfer cross-sections are small, so the decay rates k_b^+ and k_b^- are taken to be much faster than the other rates. Under this assumption, we can find the three observable rates for the four level system to second order in $(k_b^\pm)^{-1}$

$$k_1 \approx \frac{k_L^+(k_E^+ - k_g^+)}{k_b^+} + \frac{k_L^-(k_E^- - k_g^-)}{k_b^-} + k_g^+ + k_g^-$$

$$k_2 \approx k_b^+ + k_E^+ + k_L^+ - \frac{k_L^+(k_E^+ - k_g^+)}{k_b^+} \quad (4)$$

$$k_3 \approx k_b^- + k_E^- + k_L^- - \frac{k_L^-(k_E^- - k_g^-)}{k_b^-}$$

Here it is important to note that, if the photon excitation energy greatly exceeds the zero-point level of the electronic state associated with (DA)*, $k_E^\pm$ is likely to be enhanced by vibrational heating effects. In such a situation, $k_b^\pm$ can be interpreted as the sum of the nonreactive decay rates (i.e., the rate of electronic and vibrational decay to the initial thermalized ground state). When the ground-state barriers are high, $k_g^\pm$ are so slow (≈ 0) that they can be ignored and k_1 depends linearly on photon flux (via $k_L^\pm$). Since we find experimentally that the photoreduction rate changes linearly with photon flux and no "dark" back reaction is observed, we assume that the terms involving $k_g^\pm$ are negligible and take $k_E^\pm$ and $k_b^\pm$ to be independent of laser flux (at least for the cw experiments).

In general, we have

$$N_R(t) = N_R(\infty)(1 + c_1 e^{-k_1 t} + c_2 e^{-k_2 t} + c_3 e^{-k_3 t}) \quad (5)$$

The rates k_2 and k_3 are dominated by $k_b^\pm$ and are much larger than k_1, so $e^{-k_2 t}$ and $e^{-k_3 t}$ in eq 5 diminish very rapidly compared with $e^{-k_1 t}$. Therefore, at longer times, the process can be described by

$$N_R(t) \approx N_R(\infty)(1 - e^{-k_1 t}) \quad (6)$$

where we have already taken into account the initial condition $N_R(0) = 0$ (i.e., the data extrapolate smoothly to $N_R(0) \sim 0$ so that $c_1 \sim -1$ and $c_2 + c_3 \sim 0$).

This suggests that, for measurements on time scales longer than the excited-state decay, $k_b^\pm$, the four level sequential transfer model simplifies to a two level system. The experiments appear to satisfy this condition, and the data are fit by the effective two level system fairly well. The final solution for $N_R(t)$ is written as

$$N_R(t) \approx \frac{k_R}{k_R + k_0}(1 - e^{-(k_R + k_0)t}) \quad (7)$$

where k_R is the observed photoreduction rate, $k_R \simeq k_L^+ k_E^+ / k_b^+$, and k_0 is the photooxidation rate, $k_0 \simeq k_L^- k_E^- / k_b^-$. Since $k_b^\pm$ is large, the intermediate state populations $N_0^*(t)$ and $N_R^*(t)$ are very small and $N_0(t) \approx 1 - N_R(t)$. The above analysis requires that the quantum yield for electron transport, $Y = k_E^+/(k_E^+ + k_b^+)$, be much less than unity. We will use the effective two level model to analyze the data because it describes the experimental observations and is compatible with a variety of sequential electron transfer models when $k_b^\pm$ is large.

Observations on shorter time scales and at higher sensitivity are needed to determine if the other rates (k_2 and k_3), associated with the sequential electron transfer model, can be observed. Unfortunately, the rapid decay associated with $k_b^\pm$ makes their amplitudes small and their detection difficult. If the electron transfer proceeds via second-order superexchange coupling,[31-34] no intermediate $(D^+A^-)^*$ state population is created, and we expect only one additional rate to appear at short times. More detailed studies are needed to discriminate between sequential and superexchange coupling.

Additional complications need to be considered in the photoreduction of metMb and cytochrome P450, where the conditions involve the presence of the diatomic CO ligand. The experiments can still be described by a two level system, since the reduced proteins bind CO rapidly (and essentially irreversibly) on the time scale of the photoreduction. However, in these cases N_R corresponds to the fractional population of the CO bound protein, and k_0 stands for a more complex process involving both photolysis and photooxidation.

To conclude this section, we develop expressions that approximate the frequency (wavelength) dependence of the photoreduction (or photooxidation) cross-section. In general we must consider the effect of allowing a significant portion of the photon energy ($h\nu$) to redistribute in a vibrational subspace of (DA)*. Here we assume that the vibrational redistribution is rapid[35,36] compared to the transport rates and that the reaction coordinates are included within the transiently heated vibrational subspace. Under these conditions, (DA)* can be vibrationally hot and highly reactive on a time scale characterized by $(k_b^+)^{-1}$, where k_b^+ is the overall decay rate (cooling and/or electronic decay) of the reactive state. The "excess" energy available for vibrational heating in (DA)* is given by $h\nu - \Delta E$, where ΔE can have a variety of interpretations (e.g., the zero-point energy of the electronic state associated with (DA)*, the energy loss due to photochemical reactions such as bond photolysis, the dissipation of energy into a vibrational subspace that is not associated with the reaction coordinate, etc.). The photoreduction rate is given as before by

$$k_R = \frac{k_L^+ k_E^+}{k_b^+} \quad (8)$$

where explicit frequency dependence is found in the photoexcitation rate, k_L^+, through the absorption cross-section $\sigma_d^+(\nu)$ (see eq 3). Additional wavelength dependence can, in principle, be carried by the excited state transport rate

$$k_E^+(\nu) \simeq k_0 \exp\left(-\frac{E_A}{k_B T^*}\right) \quad (9)$$

where the rate is approximated by an Arrhenius expression having a barrier, E_A, and a prefactor, k_0. After absorption of a single photon, the vibrational temperature,[37] prior to cooling and relaxation to the ground state, is given by

$$T^* = \frac{(h\nu - \Delta E)}{C_v} + T_0 \quad (10)$$

where T_0 is the equilibrium (or photostationary state) temperature of the system. In these expressions, ν is the photon frequency, and $\sigma_d^+(\nu)$ is a (weak) absorption cross-section, centered at ν_0, which is a "doorway" to (DA)*. If ν_0 is assumed to be relatively far removed from the optical frequencies employed in the experiments, we can approximate σ_d^+ using a Lorentzian line shape and note that $\sigma_d^+ \sim \nu$ if $\nu_0 \gg \nu$ and $\sigma_d^+ \sim \nu^{-1}$ if $\nu_0 \ll \nu$. The transient heating of the (DA)* vibrational subspace is described by T^* and is dependent upon the photon energy, the vibrational specific heat, C_v, and the energy loss, ΔE.

Under pulsed laser irradiation, the photoexcitation rate of a single chromophore can be relatively high for the duration of the pulse ($\sim$10 ns) so that the "equilibrium" vibrational temperature of the absorbing species must be evaluated under photostationary state conditions.[30] We denote the photostationary temperature of the chromophore (DA complex), averaged over the laser pulse,

(31) Marcus, R. A. *Chem. Phys. Lett.* **1987**, *133*, 471.
(32) Bixon, M.; Jortner, J.; Michel-Beyerle, M.; Ogrodnik, A.; Lersh, W. *Chem. Phys. Lett.* **1987**, *140*, 626.
(33) Hu, Y.; Mukamel, S. *Chem. Phys. Lett.* **1989**, *160*, 410.
(34) Islampour, R.; Lin, S. H. *J. Phys. Chem.* **1991**, *95*, 10261.
(35) Miller, R. D. *Annu. Rev. Phys. Chem.* **1991**, *42*, 581.
(36) Elsaesser, T.; Kaiser, W. *Annu. Rev. Phys. Chem.* **1991**, *42*, 83.
(37) Henry, E.; Eaton, W.; Hochstrasser, R. *Proc. Natl. Acad. Sci. U.S.A.* **1986**, *83*, 8982.

as $\langle T^* \rangle$ and recognize that it will depend upon the details of the bleaching recovery and the coefficients of thermal transport within the medium.[30] This increase in average chromophore temperature ($T_0 < \langle T^* \rangle < T^*$) can potentially lead to enhanced electron transport in pulsed laser experiments, since T_0 must be replaced by $\langle T^* \rangle$ in eq 10.

When the wavelength dependence of the photoreduction cross-section ($\sigma_R = k_R/J$) is dominated by the transport rate, we can write

$$\sigma_R(\lambda) = A_1 \exp\left\{-\frac{A_2\lambda}{1 - A_3\lambda}\right\} \tag{11}$$

where $\lambda = c/\nu$ is the photoreduction wavelength and the fitting parameters are given by

$$A_1 = \frac{k_0}{k_b^+}\sigma_d^+$$

$$A_2 = \frac{E_A C_v}{hck_B} \tag{12}$$

$$A_3 = \frac{\Delta E - C_v T_0}{hc}$$

In the expression for A_1, we have implicitly neglected the wavelength dependence carried by σ_d^+, since for nonresonant conditions it will scale as $\nu^{\pm 1}$ and be much weaker than the exponential behavior governed by A_2 and A_3.

To obtain the more traditional model of excited-state electron transport, the optical transition is assumed to be resonant so that the wavelength dependence of the cross-section is carried by $\sigma_d^+(\nu)$ in the limit of no transient heating ($C_v \rightarrow \infty$). It turns out that a Lorentzian absorption line shape is not able to reproduce the experimentally observed frequency dependence of $\sigma_R(\nu)$. However, when a Gaussian line shape is used, the following wavelength dependent function adequately describes the data.

$$\sigma_R(\lambda) = B_1 \exp\left\{-B_3\frac{(1 - B_2\lambda)^2}{\lambda^2}\right\} \tag{13}$$

with fitting parameters given by

$$B_1 = \sigma_d^+(\nu_0)\frac{k_E^+}{k_b^+}$$

$$B_2 = \frac{\nu_0}{c} \tag{14}$$

$$B_3 = \frac{c^2}{2\sigma^2}$$

where ν_0 and σ are the Gaussian position and bandwidth, respectively (expressed in Hz, with c as the speed of light). In this limit, k_E^+ is assumed to depend only upon the equilibrium temperature of the surroundings, so that there is no additional wavelength dependence in σ_R. It should be understood that, under the most general circumstances, the wavelength dependence of σ_R can arise from both k_E^+ and σ_d^+. We will use eqs 11–14 as approximations for testing the two limiting cases of the simple model presented above.

III. Materials and Methods

Horse heart myoglobin (type III), cytochrome c (type VI), and heme octapeptide are purchased from Sigma Chemical Company and used without further purification. The buffers are potassium phosphate (0.1 M, pH 7) or citrate/phosphate (0.1/0.2 M, pH 7). Glycerol mixtures are made using spectrophotometric grade glycerol (99.5%, Aldrich). Ferricyanide is added to cytochrome c to make sure that all the cytochrome c is in the ferric state before it is photoreduced. Since ferricyanide has been reported[38] to block the photoreduction of cytochrome c, excess ferricyanide is extracted by using a refrigerated centrifuge (Sorvall RT6000B) with a microconcentrator (Centricon-30, 30,000 MW cutoff). Samples of ferrocytochrome c for direct photooxidation are prepared in 0.1 M phosphate buffer by addition of sodium dithionite followed by centrifugation to remove excess reductant and deoxygenation with argon gas. The heme octapeptide (10 μM) is complexed with methionine (2.5 M, pH 7.2) or histidine (0.1 M, pH 7) in order to eliminate aggregation effects. The methionine (2.5 M) solution is prepared according to the method of Yang by adding a solution of 6 M KOH in 0.1 M phosphate buffer to solid L-methionine until it reaches neutral pH. The desired concentration is obtained by adjusting the volume with 0.1 M phosphate buffer, pH 7.0.[39] Cytochromes $P450_{cam}$ and b_5 are provided by Prof. S. G. Sligar (U. of Illinois). Cytochrome $P450_{cam}$ (m^{os}) is produced using *E. coli*[40] and dissolved in 0.05 M Tris buffer with 0.1 M KCl and saturated with camphor (pH 7.2).

For kinetic measurements, the typical protein concentrations are ~10–20 μM. The samples are sealed in quartz cuvettes (5 × 10 mm^2 cross-section) and then flushed with pure dry argon gas to remove oxygen. Deoxygenated metMb solutions are equilibrated with CO because photoreduced metmyoglobin binds CO to form MbCO, which is very stable at room temperature. Typical concentrations for the Raman measurements are ~42 and ~60 μM for myoglobin and cytochrome c, respectively. The sample is sealed in either a 5 × 10 mm^2 cross-section quartz cuvette or a spinning quartz cell and prepared as for the kinetic measurements.

In the low-temperature absorption measurement of photoreduced MbCO, a mixture of 75% glycerol and 25% aqueous buffer is used. The solution is equilibrated with CO for ~1 h because the high viscosity of glycerol slows down the diffusion of CO into the solution. The sample is placed in a copper cell with two quartz windows, and the cell is mounted on the cold finger of a CTI Cryogenics (Model 22C) cooling system with a closed cycle helium refrigerator. A TRI Research T-200 Cryogenic Controller unit is utilized to monitor and regulate temperature.

The protein is photoreduced by laser illumination at various wavelengths, and its optical spectrum as a function of time is probed using a quartz lamp (GE) and a double monochromator (Spex) with a photomultiplier (R955, Hamamatsu) connected to a lock-in amplifier (5101, Princeton Applied Research). The data are digitized using an A/D converter and a personal computer. The absorption spectrum before and after the sample is reduced is recorded by a Perkin-Elmer spectrophotometer (Model 320) interfaced to a personal computer.

The photoreduction and photooxidation cross-sections, $\sigma_R(\lambda)$ and $\sigma_0(\lambda)$, are defined by

$$\sigma_R(\lambda) = \frac{k_R(\lambda)}{J} \tag{15}$$

$$\sigma_0(\lambda) = \frac{k_0(\lambda)}{J} \tag{16}$$

where J is the average photon flux (photons/cm^2 s) incident on the sample molecules and λ is the laser wavelength. Due to the absorption of light by the sample, the photon flux decays according to Beer's Law along the light path. Taking this into account, the value of J is found from the incident flux, J_0, by averaging the photon flux over the light path in the sample

$$J = \frac{1 - 10^{-\epsilon cl}}{\epsilon cl \ln 10} J_0 \tag{17}$$

where ϵcl is the standard optical density, measured using a

(38) Vorkink, W. P.; Cusanovich, M. A. *Photochem. Photobiol.* **1974**, *19*, 205.
(39) Yang, E. K. Ph.D. Thesis, U. Cal. Berkeley, 1979.
(40) Wells, A.; Li, P.; Champion, P. M.; Martinis, S. A.; Sligar, S. G. *Biochemistry* **1992**, *31*, 4384–4393.

spectrophotometer. (c is concentration, l is pathlength, and ϵ is extinction coefficient of the absorbing molecules).

Several laser lines are used in the kinetic measurements to obtain the wavelength dependence of the photoreduction and photooxidation cross-sections. Ultraviolet wavelengths are mainly from a Coherent Ar^+ laser (Innova 100) and the visible lines are from a dye laser (CR-599, Coherent) containing Stilbene III (Exciton) and pumped by an Ar^+ laser. A mercury lamp (15 W, UF-4-H, American Ultraviolet Co.) is used at 254 nm. Prisms are utilized to separate the multiple UV lines of the Ar^+ laser, and all the laser beams are expanded to produce uniform power over the sample area. In this way an accurate measurement of the incident laser photon flux, J_0 (photons/s-cm^2), could be obtained. Powers passing through a fixed aperture (1.72 cm^2) next to the sample surface are measured with a Coherent 210 power meter and a Liconix (35PM-1) power meter, and the latter is calibrated by the former. Typical values for the incident flux are 5.4×10^{14} photons/s-cm^2 at 254 nm, 1.2×10^{17} photons/s-cm^2 at 334.5 nm, 2.7×10^{17} photons/s-cm^2 at 363.8 nm, and 3.6×10^{16} photons/s-cm^2 at 420 nm.

Raman spectra are recorded using a triple grating spectrograph (Spex, Inc.) equipped with a 2400 g/mm grating and an optical multichannel analyzer (Princeton Instruments). CW excitation is provided by a Coherent dye laser (Stilbene III) pumped by an Ar^+ laser, and pulsed excitation is provided by a Lumonics dye laser (HyperDYE-300) containing bis-MSB dye (Exciton) and pumped by a XeCl excimer laser (EMG 53 MSC, Lambda Physik).

IV. Results and Discussion

Structural Comparisons. In order to characterize the photoreduced heme proteins, we compare the photoreduced product and the chemically reduced samples using absorption and resonance Raman spectra. Typical absorption spectra of metmyoglobin and ferricytochrome c, and their photoreduced and chemically reduced products, are shown in Figure 2. In these examples, the sample is photoreduced with laser illumination at $\lambda = 363.8$ nm. The direct chemically reduced sample is made from the same ferric solution as used in the photoreduction experiment in order to compare the optical density of sample on an absolute scale. The photoreduced and chemically reduced spectra have slightly different line shapes and peak heights for both samples. Additional chemical reductant (sodium dithionite for Mb and L-ascorbic acid for cytochrome c) is also added to the photoreduced products to see if they can be further reduced.

In the metMb/CO case (top panel of Figure 2), the photoreduced MbCO has a wider Soret band (solid line), and the addition of dithionite compresses the blue side of Soret band (dotted line) and makes it similar to the chemically reduced sample (dashed line). This implies that the photoreduction is incomplete, possibly due to photolysis and photooxidation back-reactions in the laser beam. However, the red side of the Soret band remains different from the chemically reduced species even after dithionite is added. At very low temperature (10 K), the spectral comparison also shows clearly that the red side of the Soret band of photoreduced MbCO remains much broader than the chemically reduced sample (insert of Figure 2). We have previously observed a dramatic narrowing of the MbCO Soret band at low temperature[41] and assigned it to the freezing out of torsional motions of the bound CO.[42] The insert of Figure 2 shows that, even at 10 K, the red edge of the photoreduced MbCO remains much broader than the chemically reduced species and indicates that photoinduced distal pocket modifications, enhancing the coupling of the bound CO torsional modes, are not responsible for the extra broadening at room temperature.[42] Notice, however, that the red edge of the

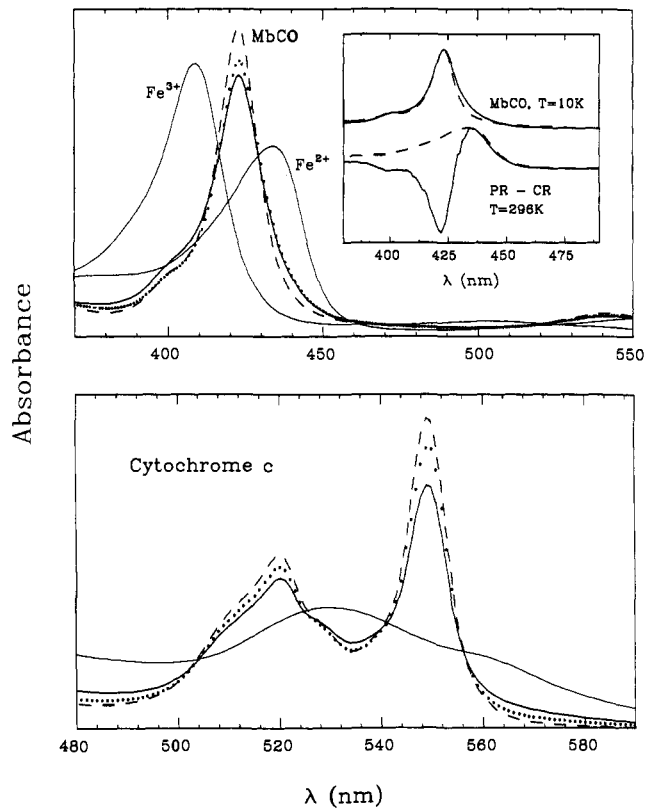

Figure 2. Top panel: Comparisons of Soret band of photoreduced and chemically reduced MbCO. Solid line: photoreduced (363.8 nm) MbCO. Dotted line: photoreduced sample after adding dithionite. Dashed line: chemically reduced MbCO (using dithionite). Fe^{3+} and Fe^{2+} indicate the Soret band of metmyoglobin and deoxymyoglobin, respectively. Insert: comparisons between photoreduced (solid) and chemically reduced (dashed) MbCO at 10 K. The sample is in a mixture of 75% glycerol and 25% aqueous phosphate buffer. The peaks are normalized for easy comparison, and the difference between the photoreduced (PR) and chemically reduced (CR) MbCO spectra at 296 K is also shown and compared to the deoxy Mb spectrum (dashed line). Lower panel: Comparisons of α and β bands of photoreduced and chemically reduced cytochrome c. Solid line: photoreduced (363.8 nm) cytochrome c. Dotted line: the same sample after adding ascorbate. Dashed line: chemically reduced cytochrome c.

MbCO Soret band corresponds to the peak of the Soret band of deoxymyoglobin. This suggests an alternative explanation, where the broadening of the photoreduced MbCO Soret band is actually due to a small population of deoxy Mb, modified as a result of the illumination, which cannot bind CO. From the difference spectra (photoreduced minus chemically reduced), we extract a peak position that corresponds to deoxy Mb (434 nm). The lineshape of the difference spectrum is also similar to that of native deoxy Mb (insert of Figure 2).

Resonance Raman (RR) spectroscopy can be used for fine structure studies of photoreduced heme proteins by comparing the RR spectra of the photoreduced and chemically reduced species. The Raman spectral comparison for MbCO (Figure 3, top panel) shows that a shoulder near 490 cm^{-1} appears on the low-frequency side of the Fe–CO stretching mode (509 cm^{-1}). This is the major difference between the Raman spectra of photoreduced and chemically reduced MbCO. Notice the similarity between the spectra of the photoreduced sample and that of the sample at low pH (pH 4.5). The appearance of the mode at $\sim$490 cm^{-1} suggests that a protein residue in the distal pocket may be modified upon photoreduction.[43] The presence of the 252-cm^{-1} mode in all spectra indicates that the proximal conformation, which dictates the relative orientation and inter-

(41) Šrajer, V.; Schomacker, K. T.; Champion, P. M. *Phys. Rev. Lett.* **1986**, *57*, 1267.
(42) Šrajer, V.; Champion, P. M. *Biochemistry* **1991**, *30*, 7390.
(43) Morikis, D.; Champion, P. M.; Springer, B. A.; Sligar, S. G. *Biochemistry* **1989**, *28*, 4791.

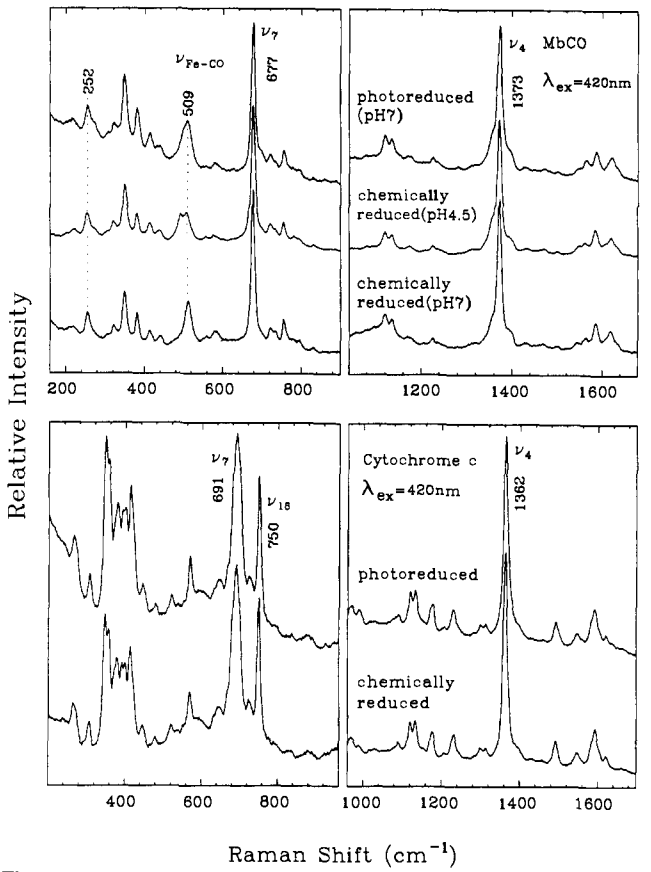

Figure 3. Top panel: Resonance Raman spectrum (λ_{ex} = 420 nm) of photoreduced MbCO (λ = 363.8 nm, pH 7) and chemically reduced MbCO (pH 7) in a spinning cell. The major difference is a shoulder near 490 cm^{-1} on the low-frequency side of the Fe–CO stretching mode (509 cm^{-1}). This is similar to the low pH spectrum (pH 4.5, see plot) and suggests that the distal pocket may be modified. Lower panel: Raman spectra (λ_{ex} = 420 nm) for chemically reduced and photoreduced cytochrome *c* (λ = 363.8 nm). There is no noticeable difference between the two spectra.

action of HisF8 and the heme, is preserved.[44,45] All the observations taken together suggest that only slight modifications of the myoglobin distal pocket occur during the laser irradiation and photoreduction process.

For cytochrome *c* (Figure 2, bottom), we display the α–β bands, which are very sensitive to the oxidation state. The line shape of the α band in the photoreduced cytochrome *c* (prepared at 363.8 nm) is not altered, but the peak height is lower compared to the chemically reduced protein. Even after ascorbate is added to the photoreduced cytochrome *c*, the peak height still remains smaller than that of native ferrocytochrome *c*. We attribute this to a small amount of protein denaturation during the laser illumination. This type of denaturation is also observed in myoglobin. The Raman spectrum of photoreduced cytochrome *c* (Figure 3, lower panel) does not show any significant differences from that of chemically reduced cytochrome *c*. The absorption spectrum of cytochrome *c* after photoreduction and reoxidation is quite similar to that of the original oxidized sample. In particular, we do not see the loss of intensity in the 695-nm band reported by Bartocci et al.[18] and attributed to alteration of the axial methionine ligand. The photoreduction cross-section of the reoxidized protein solution is identical within error to that of the original sample.

Kinetics Experiments. Kinetics experiments are carried out to extract the photoreduction cross-section using eqs 7 and 15. The

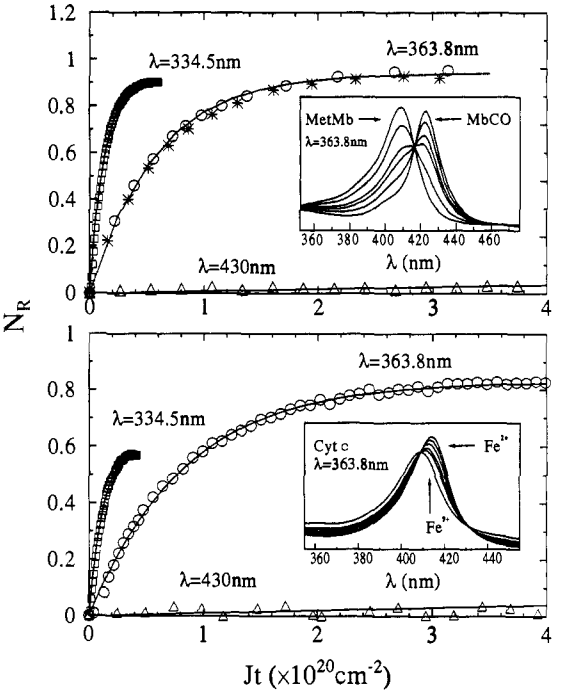

Figure 4. Kinetic measurements of photoreduction. $N_R(t)$ increases with irradiation time and is fit by eq 7 at the different wavelengths. The top panel is for Mb and the lower panel is for cytochrome *c*. The time is rescaled using the photon flux in order to compare the photoreduction cross-sections at different wavelengths. Notice that for myoglobin there are two sets of data shown for λ = 363.8 nm. The open circle is a typical photoreduction measurement. The * indicates a sample that has been reoxidized and then photoreduced at the same wavelength. Insert: typical changes of the absorption spectra with illumination time. For Mb in the presence of CO, the shift of the Soret band indicates that metMb is converted into MbCO. For cytochrome *c*, the Soret and α and β bands (not shown) demonstrate that the ferric sample is reduced to the ferrous state. Parameters used in the fits: for Mb/CO λ = 363.8 nm, σ_R = 1.2 × 10^{-20} cm^2; σ_0 = 9.8 × 10^{-22} cm^2; λ = 334.5 nm, σ_R = 7.4 × 10^{-20} cm^2; σ_0 = 4.6 × 10^{-21} cm^2; λ = 430 nm, σ_R = 1.7 × 10^{-22} cm^2. For cytochrome *c*, λ = 363.8 nm, σ_R = 7.9 × 10^{-21} cm^2, σ_0 = 1.5 × 10^{-21} cm^2; λ = 334.5 nm, σ_R = 7.2 × 10^{-20} cm^2, σ_0 = 3.5 × 10^{-20} cm^2; λ = 430 nm, σ_R = 1.1 × 10^{-22} cm^2.

transient optical decay, $\Delta A(t)$, is recorded as a function of illumination time at a given wavelength and converted to $N_R(t)$ using absorption spectra measured before and after photoreduction. The absorption spectrum of the chemically reduced protein is used as a standard to gauge 100% reduction. Typical data for metMb/CO and cytochrome *c* at three different photoreduction wavelengths are shown in Figure 4. The solid lines are produced by fitting the data with eq 7 in order to determine k_R and k_0. The photoreduction and photooxidation cross-sections, σ_R and σ_0, are obtained from eqs 15 and 16 and the measured photon flux, J_0. In the figures, time is rescaled by photon flux in order to compare the photoreduction cross-sections for the different wavelengths. It should be noticed that for cytochrome *c* at 334.5 nm (Figure 4, lower panel), $N_R(t)$ approaches a value that is much less than unity. This is explained by a photooxidation rate that increases more rapidly than the photoreduction rate at shorter wavelengths. As a result, more ferric molecules are present in the photostationary state (see eq 7). At still shorter wavelengths, such as 300.5 nm, only ~30% ferrocytochrome *c* is present at steady state, even though the photoreduction rate continues to increase.

In order to investigate the reversibility of the photoreduction process and to check if the slight modifications of the photoreduced myoglobin affect the mechanism of the photoreduction process, a photoreduced MbCO sample made with 363.8-nm illumination is oxidized in the air. After flushing with argon gas and equilibrating with CO, it is photoreduced again at 363.8 nm. The data are shown by the asterisks in the top panel of Figure 4. This

(44) Zhu, L.; Sage, J. T.; Rigos, A. A.; Morikis, D.; Champion, P. M. *J. Mol. Biol.* **1992**, *224*, 207–215.
(45) Wells, A.; Sage, J. T.; Morikis, D.; Champion, P. M.; Chiu, M.; Sligar, S. *J. Am. Chem. Soc.* **1991**, *113*, 9655.

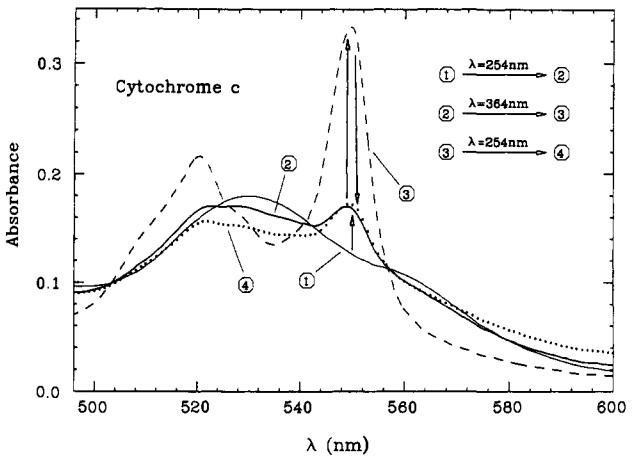

Figure 5. The change of α and β band of cytochrome *c* under different wavelengths of illumination. First we use 254 nm to reduce ferricytochrome *c*. Only a small part of the sample is reduced ([1] → [2]). Then 363.8 nm excitation is used to reduce it again ([2] → [3]). We can see there is a big change, indicating much more photoreduction. Finally, we again apply 254-nm irradiation and photooxidize the sample ([3] → [4]). This demonstrates clearly that the photoreduction and photooxidation processes exist simultaneously and that the 254-nm radiation enhances the photooxidation process.

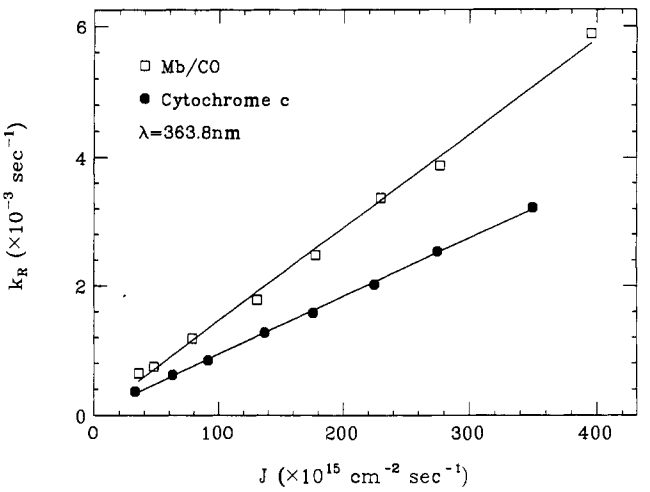

Figure 6. Photoreduction rate (k_R) vs photon flux. Both myoglobin and cytochrome *c* have good linearity over at least an order of magnitude of photon flux.

result indicates that the photoreduction process is reversible, and the kinetic mechanism is not altered.

In the insert windows of Figure 4, typical changes of the absorption spectra with illumination time are shown, and we see that good isosbestic points are obtained in both metMb/CO and cytochrome *c*. The red-shifted Soret band is increasing in both samples during the time course of laser irradiation, indicating that the ferric heme is being converted into the ferrous form and that the two-state model is a good approximation.

We also observe that photoreduction using visible radiation (~430 nm) does not lead to fully reduced samples. Since the rates are so slow at these wavelengths, oxygen may leak into the samples, preventing the proteins from being completely photoreduced at longer wavelengths.

In order to check on the spontaneous autooxidation rates, the oxidation of photoreduced MbCO and cytochrome *c* samples (kept anaerobically in the dark) was monitored over very long time scales. These measurements demonstrate that, in the absence of photons, there is no significant oxidation on the experimental time scale (i.e., k_g^- can be neglected in the expression for k_0 and, since $k_g^- > k_g^+$, k_g^+ can also be neglected in the expression for k_R).

In the case of cytochrome *c*, we can independently verify that the back reaction is dominated by photooxidation. Figure 5 demonstrates how the α and β bands of cytochrome *c* change with different illumination wavelengths. First, ferricytochrome *c* is irradiated with 254-nm radiation, and only a very small increase of the α and β bands is observed because of the photooxidation process (i.e., a significant amount of ferricytochrome *c* is present in the steady state). Then 363.8-nm radiation is used to reduce the sample further. The large absorbance change means that much less of the ferric material is present in the steady state when the longer wavelength illumination is used. Finally, the sample is irradiated again using the 254-nm line, and photooxidation takes place.

This sequence of irradiation at different wavelengths shows clearly that photoreduction and photooxidation processes exist simultaneously and that the photooxidation rate increases more rapidly than the photoreduction rate at shorter excitation wavelengths. Note that after the second application of 254-nm illumination, the background of the absorption spectrum is noticeably changed. We suspect that this is due to photon-induced sample denaturation at 254 nm that takes place along with the photoreduction and photooxidation processes. As gauged by the small increases in broad background absorption, denaturation also takes place at 275 and 363.8 nm but much less extensively (data not shown). In the metMb/CO samples, the steady state shows more photoreduction (MbCO) than ferricytochrome *c* samples, probably due to the rapid CO binding to iron, which stabilizes the photoreduced state and minimizes the photon driven back-reaction. At 254 nm, the photoreduction rate of metMb/CO is tremendously enhanced, and approximately 70% of the system is found as MbCO in the steady state.

Cross-Section Determination. In order to extract a photoreduction cross-section, σ_R, from the data using eq 15, the photoreduction rate, k_R, must be shown to be proportional to the photon flux. The photon flux dependence of the photoreduction rate is measured and displayed in Figure 6, which shows good linearity for both metMb/CO and cytochrome *c*. Additional studies, using pulsed irradiation at 420 nm, also demonstrate linearity up to the point where ground-state bleaching leads to differential saturation of the oxidized and reduced Raman signals (P. Li, unpublished observations). We also find that the cross-section measured under 308-nm illumination with a train of unfocused 10-ns pulses ($J_0 \sim 4 \times 10^{23}$ photons/s-cm^2) is identical within error to that measured under cw illumination at 301 nm ($J_0 \sim 4.5 \times 10^{16}$ photons/s-cm^2). This eliminates the possibility that two-photon processes dominate the photoreduction mechanism, contrary to the conclusions of Masuda et al.[20] Therefore, the photoreduction cross-section, σ_R, defined in eq 15 reflects the intrinsic probability for a one-photon reduction of the heme proteins under study. The invariance of the steady-state populations as a function of flux demonstrates that k_0 is also linearly dependent on J.

The wavelength dependence of the photoreduction cross-section is shown in the upper panel of Figure 7. Although measurable photoreduction occurs under intense illumination at $\lambda > 400$ nm, σ_R increases dramatically under UV illumination. The increase of σ_R in the UV is somewhat less for cytochrome *c* than for Mb. The roughly exponential increase in σ_R and σ_0 at shorter wavelengths is surprising, since it does not show resonance behavior coincident with the Soret band, underlying visible charge-transfer bands, or the near ultraviolet absorption bands of aromatic amino acids, as might be expected for excited-state electron transfer. However, the data are compatible with the traditional model of excited-state transport, eq 13, if $\sigma_d^+(\nu)$ is centered further to the ultraviolet ($\nu_0 \sim$ 250–260 nm, dashed lines in Figure 7). Alternatively, the data can be well fit using a model that approximates the effects of transient vibrational heating, and the solid curves are fits using eq 11. The fitting parameters for the photoreduction of cytochrome *c* and metMb/CO are listed in

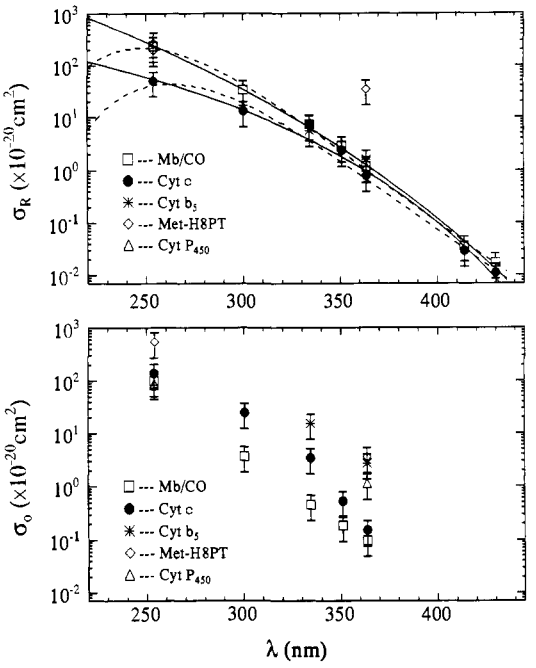

Figure 7. Top panel: wavelength dependence of the photoreduction cross-section on a semilogarithmic scale. Although measurable photoreduction occurs for $\lambda > 400$ nm, σ_R increases dramatically for $\lambda < 400$ nm. The solid and dashed curves result from fitting the data using eqs 11 and 13, respectively. Lower panel: wavelength dependence of the photooxidation cross-section obtained from the same experimental data as in the top panel. σ_0 increases slightly faster than σ_R with decreasing wavelength.

Table I. Fitting Parameters for $\sigma_R(\lambda)$[a]

	A_1	A_2	A_3	σ_d^+ [b]	E_A [c]	ΔE [c]
Mb/CO	230	19	1.2	~1	10.5	4.5
cyt *c*	2.6	9	1.6	~0.01	7.2	4.7
	B_1	B_2	B_3	$\sigma_d^+(\nu_0)$ [d]	ν_0	σ
Mb/CO	0.22	4.0	3.2	2	1.2	0.12
cyt *c*	0.044	3.8	3.7	0.4	1.1	0.11

[a] Units for various parameters in this table are A_1 and B_1 (10^{-17} cm^2); A_2, A_3, and B_2 (10^{-3} nm^{-1}); B_3 (10^6 nm^2); σ_d^+ (10^{-17} cm^2); E_A (kcal/mol); ΔE (10^{-19} J); ν_0 and σ (10^{15} Hz). [b] Depends on the ratio $k_0/k_b^+ \sim 10^{13}/10^{11} \sim 10^2$. [c] Depends on C_v. Following ref 30, we take $C_v \sim 7 \times 10^{-22}$ J/K for Mb and 5×10^{-22} J/K for cytochrome *c*. [d] Quantum yield is assumed to be $Y = k_E^+/k_b^+ \sim 0.1$.

Table I. Values of σ_d^+, ν_0, σ, E_A, and ΔE based on estimates of C_v and k_0/k_b^+ are also included.

In order to connect the photoreduction cross-section to the quantum yield, Y, one should calculate the ratio $\sigma_R(\nu)/\sigma_d^+(\nu)$, where $\sigma_d^+(\nu)$ is the component of the total absorption cross-section at the photoreduction wavelength that produces the reactive state $(DA)^*$. This ratio is unknown for the proteins in this study, since the strong optical transitions of the heme and amino acid chromophores can obscure the relatively weak underlying absorbance due to $\sigma_d^+(\nu)$. Many workers simply define Y as $\sigma_R(\nu)/\sigma_A(\nu)$, where $\sigma_A(\nu)$ is the full absorption cross-section of the sample. It is important to realize that such a definition is useful only when $\sigma_R(\nu)$ and $\sigma_A(\nu)$ have the same wavelength dependence and Y is constant. Figure 7 demonstrates that σ_R has a very different wavelength dependence than σ_A, so that Y cannot be defined with certainty. For example, if we take σ_d^+ to be $\sim 10^{-17}$–10^{-18} cm^2 in the region between 200 and 500 nm, Y will vary from 10^{-1} to 10^{-4}. (Note that the heme absorption cross-sections at the Soret maxima are 1.45×10^{-16} cm^2 for met Mb and 1.6×10^{-16} cm^2 for ferricytochrome *c*.)

The error bars shown in Figure 7 are estimated from the standard deviation of σ_R measured 15 times at $\lambda = 363.8$ nm. A larger error is assigned to σ_R at 254 nm due to the difficulty of measuring and calibrating the photon flux. The determination of σ_R in the visible wavelength range is also subject to larger error, since the photoreduction rate is estimated from the initial slope of $N_R(t)$ to eliminate long term artifacts arising from oxygen leakage, etc.

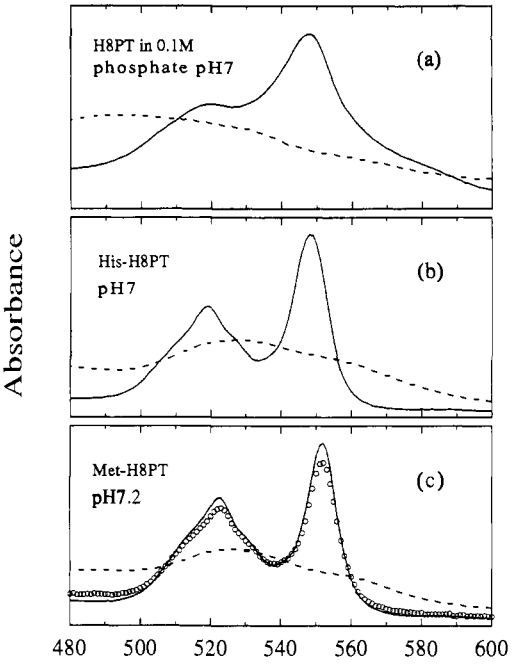

Figure 8. Optical spectra of 10 μM H8PT in (a) 0.1 M phosphate buffer, pH 7; (b) 0.1 M His with 0.1 M phosphate buffer, pH 7; (c) 2.5 M Met, pH 7.2. Dashed line, ferric heme; solid line, ferrous, chemically reduced by dithionite. Circles in (c): photoreduced at 363.8 nm.

Heme Octapeptide. We have attempted to determine the role of the protein as an electron donor by excluding most of the amino acid residues. The model compound used for this purpose was heme octapeptide (H8PT), obtained from proteolytic digestion of cytochrome *c*. The heme group of H8PT is covalently attached to an eight residue peptide (Cys-Ala-Gln-Cys-His-Thr-Val-Glu) through the two thioether linkages (Cys-14 and Cys-17) and the axial iron ligation to His-18. This arrangement partially replicates the local ligand environment of the heme proteins under investigation but eliminates the bulk of the protein material.

Heme octapeptide is known to aggregate in neutral aqueous solution.[46,47] To eliminate the aggregation, which significantly reduces the value of H8PT as a model compound for heme proteins, we utilized buffer solutions containing methionine (Met-H8PT), histidine (His-H8PT), imidazole (Im-H8PT), or tryptophan (Try-H8PT) in order to complex the sixth position of the heme iron. This has the advantage of minimizing the aggregation of H8PT molecules, in addition to mimicking the local iron–ligand geometry of the proteins under study.

Figure 8 shows the optical spectra between 500 and 600 nm for oxidized and reduced heme octapeptide in neutral aqueous (a), histidine (b), and methionine (c) solutions. Ferric heme octapeptide in pH 7 phosphate buffer (Figure 8a) has some high-spin character in the visible region, but significant aggregation is evidenced by two unresolved peaks in the Soret band (not shown), probably due to the intermolecular coordination between the α-amino group and the heme.[48] Figure 8b presents the absorption spectra of ferric and ferrous H8PT (10 μM) in 0.1 M His solution; the latter has features consistent with a six-coordinate

(46) Urry, D. W. *J. Am. Chem. Soc.* **1967**, *89*, 4190–4196.
(47) Aron, J.; Baldwin, D. A.; Marques, H. M.; Pratt, J. M.; Adams, P. A. *Inorg. Biochem.* **1986**, *27*, 227–243.
(48) Harbury, H. A.; Cronin, J. R.; Fanger, M. W.; Hettinger, T. P.; Murphy, A. J.; Myer, Y. P.; Vinogradov, S. N. *Biochemistry* **1965**, *54*, 1658–1664.

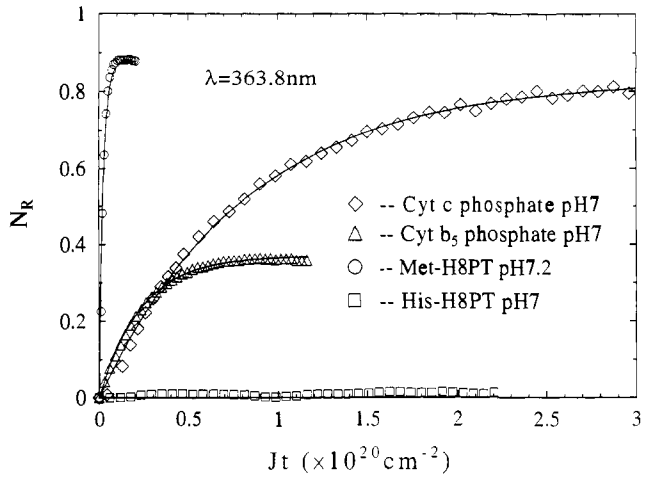

Figure 9. Comparisons of photoreduction for various heme complexes having different local ligand environments. Notice that photoreduction of heme octapeptide in 2.5 M methionine is increased by about one order of magnitude compared with cytochrome *c* in phosphate buffer. Fitting parameters: λ = 363.8 nm, for cytochrome *c*, $\sigma_R = 7.9 \times 10^{-21}$ cm²; for cytochrome b_5, $\sigma_R = 1.5 \times 10^{-20}$ cm²; for Met-H8PT, $\sigma_R = 34 \times 10^{-20}$ cm²; for H8PT with His, photoreduction process is not observed.

low-spin complex and could be an analog of cytochrome b_5. A range of H8PT concentrations between 2.5 and 120 μM in 0.1 M His solution showed no difference in the optical spectra, indicating that the aggregation has been eliminated. Imidazole[49] and tryptophan were also studied as alternative nitrogenous ligands and both show optical spectra similar to the spectra of His-H8PT. The cytochrome *c* ligation is modeled by adding methionine to a solution of H8PT to form a low-spin six-coordinate heme complex[50,51] (Figure 8c). Notice that a high concentration (2.5 M) of Met is required to form a saturated Met–H8PT complex.[39] This is due to its small equilibrium constant and the competition between ligation and aggregation.[50]

We attempted to photoreduce all of the H8PT–ligand complexes, and some of the results at 363.8 nm are compared to hemeproteins in Figure 9. The photoreduction process of Met-H8PT is faster by an order of magnitude when compared to cytochrome *c*, even though the local heme ligation is the same. It is not clear why photoreduction is so fast for Met-H8PT, although the results suggest that solution conditions and the access of solvent to the heme may play an important role. H8PT in 0.1 M phosphate buffer (pH 7) is also found to undergo photoreduction at 363.8 nm (data not shown), but aggregation effects make a quantitative measurement difficult. We estimate that the photoreduction cross section is $\sim 7 \times 10^{-21}$ cm² at 363.8 nm, which is close to the value for cytochrome *c* in the same buffer solution and at the same wavelength. The above results are inconsistent with the suggestion[20,21] that tryptophan is the sole electron donor in the photoreduction process, since there is none present in H8PT.

Another, more interesting, finding is that photoreduction of His-H8PT, Im-H8PT, and Try-H8PT is not observed at either 363.8 or 254.5 nm. The absence of photoreduction in His-H8PT is shown in Figure 9 as an example. In contrast, cytochrome b_5, which has a His-Fe^{3+}-His ligand arrangement similar to that of His-H8PT, could be photoreduced but was found to have a large photooxidation cross-section compared to cytochrome *c*. This suggests that the photoreduction and photooxidation processes are affected by the surrounding medium as well as by the details of the heme ligation state[52] and points to the possibility of multiple electron donors.

(49) Harbury, H. A.; Loach, P. A. *J. Biol. Chem.* **1960**, *235*, 3646–3653.
(50) Smith, M.; McLendon, G. *J. Am. Chem. Soc.* **1981**, *103*, 4912–4921.
(51) McLendon, G.; Smith, M. *Inorg. Chem.* **1982**, *21*, 847–850.
(52) Morikis, D.; Champion, P. M.; Springer, B. A.; Egeberg, K.; Sligar, S. G. *J. Biol. Chem.* **1990**, *265*, 12143.

Table II. Photoreduction, Photooxidation Cross-Sections, and Redox Potentials for Various Heme Systems[a]

complex	E'_0 (mV)	buffer	σ_R	σ_0	$\frac{\sigma_R}{\sigma_R + \sigma_0}$
cyt *c*	220[b]	phosphate	0.8	0.15	0.84
cyt *c*		citrate/phosphate	4.9	0.15	0.97
metMb/CO	46[b]	phosphate	1.2	0.11	0.92
metMb/CO		citrate/phosphate	2.9	0.07	0.98
cyt b_5	−7[c]	phosphate	1.6	2.7	0.37
Met-H8PT	−50[d]	2.5 M methionine	34	3.6	0.90
cyt P450	−170[e]	phosphate	1.2	1.1	0.52
Im-H8PT	~−220[d]	0.1 M imidazole	no reaction		
His-H8PT		0.1 M histidine	no reaction		
Try-H8PT		50 mM tryptophan	no reaction		

[a] σ_R and σ_0 are measured at 363.8 nm. Both are given in units of 10^{-20} cm². [b] Reference 57. [c] Reference 58. [d] Reference 48. [e] Reference 59.

Cross-Section Comparisons. Table II lists the photoreduction and photooxidation cross-sections of a variety of heme systems measured at 363.8 nm along with their corresponding redox potentials. As can be seen from the table, cytochrome *c* and myoglobin have roughly the same cross-sections for photoreduction and photooxidation, but their redox potentials differ by about a factor of 5. Similarly, the photoreduction cross-sections of Met-H8PT and cytochrome P450 differ by a factor of ~30, but their redox potentials differ by only a factor of ~3. The lack of correlation is probably due to differences between the ground- and excited-state potential surfaces as well as to the unknown redox potentials associated with the donor half-reaction ($D^+ + e^- \rightarrow D$) in either the ground or excited state.

Although time-resolved pump/probe Raman experiments on heme model compounds suggest that imidazole ligands may serve as electron donors for photoreduction,[53] another donor (or donors) must be responsible for photoreduction of cytochrome P450 (Table II and ref 21), which has cysteine rather than histidine as an axial ligand. Again, this suggests the possibility of multiple electron donors in the protein environment.

We have also studied this problem by illumination of chemically reduced cytochrome *c* at 300 nm (data not shown). This leads to a partial photooxidation of the sample with photooxidation and photoreduction rates that are very similar to those observed under illumination of the oxidized protein at this wavelength. These observations strongly suggest that the acceptor in the photooxidation process is not the oxidized donor produced by photoreduction.

This is a significant finding, since it requires charge transport into and out of the system. As noted in Section II, the scheme depicted in Figure 1 represents a "charge neutral" analysis that does not include the chemically reduced state (DA^-). The fact that the chemically reduced system has nearly identical photooxidation and photoreduction rates suggests that the state (D^+A^-) is unstable and rapidly decays to (DA^-) by accepting an electron from (or losing a proton to) the surrounding solvent. Similarly, upon photooxidation of (DA^-) to (D^-A), rapid electron loss (or proton gain) must occur with subsequent decay to (DA). This important type of "charge flow" analysis is outlined in somewhat more detail in the Appendix.

Solvent Composition and the Role of Oxygen. The effects of solvent on the photoreduction process have also been investigated. When pH 7 citrate/phosphate (0.1 M citric acid, 0.2 M KPi) or phosphate (0.1 M) buffer is used as solvent for myoglobin and cytochrome *c*, we observe a systematic difference in the photoreduction rates. The results are shown in Figure 10 where the wavelength of the photoreduction light is 363.8 nm. Notice that the photoreduction cross-section in citrate/phosphate buffer is larger than that in phosphate buffer by factors of 5 and 2.5 for cytochrome *c* and metMb/CO, respectively.

(53) Sato, S.; Kamogawa, K.; Aoyagi, K.; Kitagawa, T. *J. Phys. Chem.* **1992**, *96*, 10676.

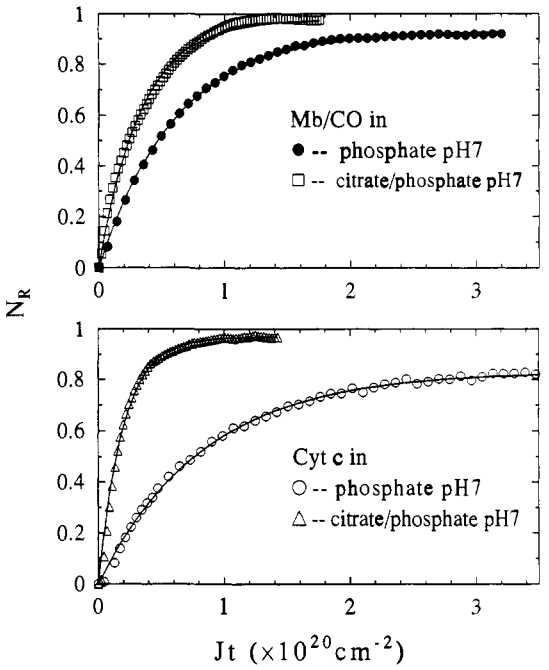

Figure 10. Comparisons of photoreduction of myoglobin (upper panel) and cytochrome *c* (lower panel) in citrate/phosphate and phosphate buffer at pH 7. The wavelength of the reducing light is 363.8 nm. The photoreduction rate apparently depends on the nature of buffer (not pH). For cytochrome *c*, the photoreduction cross section in citrate/phosphate buffer is about a factor of 5 larger than in phosphate buffer. Fitting parameters: metMb/CO at λ = 363.8 nm in phosphate buffer pH 7, σ_R = 1.2 × 10^{-20} cm^2; in citrate/phosphate pH 7, σ_R = 2.9 × 10^{-20} cm^2. Cytochrome *c* in phosphate pH 7, σ_R = 7.9 × 10^{-21} cm^2; in citrate/phosphate pH 7, σ_R = 4.9 × 10^{-20} cm^2.

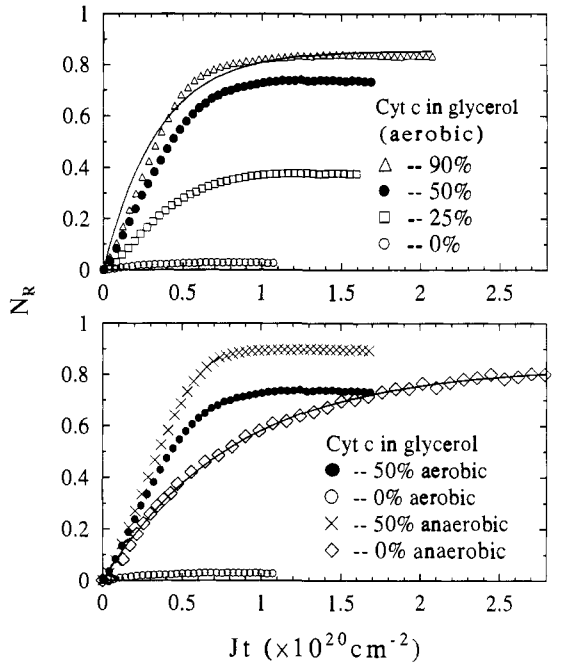

Figure 11. Top panel: The 363.8-nm photoreduction of cytochrome *c* in solutions of glycerol and phosphate buffer under aerobic conditions. The fit with a two-level model for photoreduction is not as good as in phosphate buffer. Typical behavior is shown for a 90% glycerol solution. Fitting parameters: 90% – σ_R = 2.5 × 10^{-20} cm^2, σ_0 = 4.2 × 10^{-21} cm^2; 50% – σ_R = 1.9 × 10^{-20} cm^2, σ_0 = 5.6 × 10^{-21} cm^2; 25% – σ_R = 9.0 × 10^{-21} cm^2, σ_0 = 1.3 × 10^{-20} cm^2; 0% – photoreduction process is not observed. Lower panel: comparisons of photoreduction of cytochrome *c* under aerobic and anaerobic conditions with different percentages of glycerol. Fitting parameters: for aerobic conditions, see top panel; for anaerobic conditions, 50% – σ_R = 2.5 × 10^{-20} cm^2, σ_0 = 4.0 × 10^{-22} cm^2; 0% – σ_R = 7.9 × 10^{-21} cm^2, σ_0 = 1.5 × 10^{-21} cm^2.

Next we turn to the role of dissolved oxygen. In contrast to the anaerobic conditions described above, when cytochrome *c* is dissolved in 0.1 M phosphate buffer and illuminated by 363.8-nm light under *aerobic* conditions, the protein is not photoreduced. We believe this is due to a large increase in the photooxidation rate, mediated by the presence of oxygen in the solution. A set of data for photoreduction of cytochrome *c* in various percentages of glycerol under aerobic conditions are presented in the top panel of Figure 11. These mixtures have lower oxygen content than pure phosphate buffer, since pure glycerol has only ~20% of the O_2 solubility of water.[54]

First we note that fits based on the two-level model are not as good as in pure aqueous solution. As an example, we display the fit for the 90% glycerol solution in the top panel of Figure 11. The inability of the two level model to describe the photoreduction kinetics in glycerol is probably due to the fact that glycerol, with its alcohol structure, may be involved in the photoreduction process.[26] As the glycerol percentage is decreased, the oxygen content will be increased. The parameters shown in the caption of Figure 11 indicate that the photoreduction cross-section, σ_R, is reduced by about a factor of 3, and σ_0 increases by the same factor, when the percentage of glycerol is changed from 90% to 25%. Extrapolation from published solubility measurements[54] indicates that the concentration of dissolved O_2 changes by a factor of 2.8 over this range of glycerol percentages, suggesting that the photooxidation rate is proportional to O_2 concentration.

In the lower panel of Figure 11, a direct comparison is made between the photoreduction of cytochrome *c* under aerobic and anaerobic conditions. Here we see that σ_0 in 50% glycerol is decreased (from 5.6 × 10^{-21} to 4 × 10^{-22} cm^2) in going from aerobic to anaerobic solution. This suggests that oxygen speeds up the photooxidation process but does not greatly affect the photoreduction process. On the other hand, when the cross-section of the anaerobic solution in 50% glycerol is compared to the anaerobic aqueous solution (lower panel of Figure 11), it is found that σ_R is increased ~3 times in 50% glycerol solution, while σ_0 decreased about same factor. This data strongly suggest that the alcohol group of glycerol affects the photoinduced redox reaction[26] by enhancing the photoreduction process and inhibiting photooxidation. However, due to the strong coordination sphere offered by the protein in cytochrome *c*, it seems unlikely that the mechanism involves direct coordination between the alcohol group and the heme iron as suggested for model compounds.[26] (It is of interest to note that very high alcohol concentrations have also been reported to significantly *reduce* the photoreduction rate of cytochrome *c*.[38])

Pulsed Excitation. We have also investigated the effects of pulsed laser excitation and used transient Raman spectra to probe the photoreduction process. A spinning sample is used to avoid the effects of convection, which greatly complicates the analysis. The sample spins quickly enough so that, at the 100-Hz repetition rate of the excimer laser, each 10-ns pulse probes an unperturbed portion of the sample and no thermal convection gradients are allowed to build up as happens with stationary samples. The oxidation marker band (ν_4) is monitored and used as an indication of photoreduction.

Two sets of data are shown in Figures 12 and 13 for the photoreduction of cytochrome *c* and myoglobin (without CO). The data are taken under aerobic and anaerobic conditions in both glycerol and aqueous solutions. A wavelength of 420 nm is used both as the excitation source for Raman scattering and as the photoreducing source. Due to the tightly focused 10-ns laser pulse, the photon flux is ~10 orders of magnitude larger than for the cw kinetic studies at 363.8 nm. This leads to an increase of the photoreduction rate through its dependence on

(54) Jordan, J.; Ackerman, E.; Berger, R. *J. Chem. Phys.* **1956**, *78*, 2979.

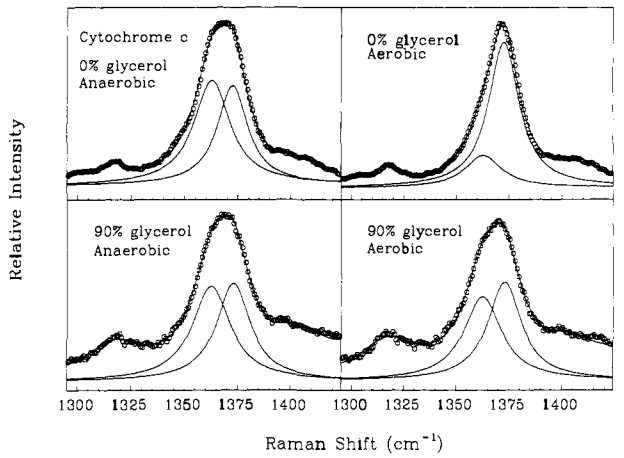

Figure 12. Photoreduction of cytochrome *c* using a focused laser beam and a spinning cell (10 ns, λ_{ex} = 420 nm). The photoreduced material in the Raman spectrum is indicated by the appearance of a new oxidation marker band, ν_4, at lower frequency. The fit using two Lorentzian line shapes is represented by the solid line.

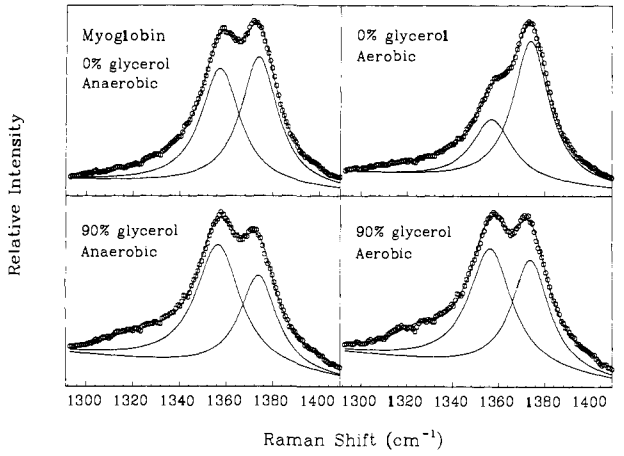

Figure 13. The same measurement and fit as in Figure 12 but for myoglobin.

k_L^+ (eq 8). The high flux can also result in an increase of the chromophore temperature[30] that can further enhance the electron-transfer rate k_E^+. The more rapid photoreduction rates allow the reduced species to be observed even on the 10-ns time scale, although photostationary state populations of the reduced species are not necessarily reached within a single pulse.

The ratio of the ν_4 Raman bands at ~1360 cm^{-1} (reduced) and ~1375 cm^{-1} (oxidized) in glycerol solution (Figures 12 and 13) is roughly the same for the aerobic and anaerobic samples, presumably due to the reduced O_2 solubility. On the other hand, in aqueous solution the ν_4 band signaling photoreduction is much smaller under aerobic conditions, due to the larger O_2 solubility and enhanced photooxidation. The reason that reduction is observed at all in the aqueous solution under aerobic conditions (it cannot be seen in cw kinetic measurements) is probably due to the fact that the Raman signal is detected during the 10-ns laser pulse and the oxygen mediated back reaction may not be completed on such a short time scale.

Finally, we can estimate a lower limit for the excited-state electron transfer rate, k_E^+, based on the assumption that $k_L^+ \sim k_b^+$, which is typical for heme systems driven into saturation.[30] Under this assumption, the photoreduced product is created only if k_E^+ is ~10^8 s^{-1}, since smaller values for k_E^+ would not allow observation of the reduced heme within a single 10 ns laser pulse. To be more quantitative, we calculate the fraction of photoreduced hemes within a single 10-ns pulse by using the resonance Raman cross-sections of the ν_4 mode[55] and the data in Figures 12 and 13. This leads directly to $k_R = 5.2 \times 10^7$ s^{-1} for metMb and $k_R = 8.3 \times 10^7$ s^{-1} for cytochrome *c*, in good agreement with the above estimate. After normalizing by the laser flux, we find the ratio of the photoreduction cross-sections in the pulsed and cw experiments at 420 nm to be $\sigma_R(pulsed)/\sigma_R(cw) \sim 1 \times 10^2$ and 2×10^2 for metMb and cytochrome *c*, respectively. If this enhancement is assumed to be due to photostationary state heating of the chromophore, we find

$$\ln\frac{\sigma_R(pulsed)}{\sigma_R(cw)} = \frac{E_A}{k_B}\left(\frac{1}{T^*_{cw}} - \frac{1}{T^*_{pulsed}}\right) \qquad (18)$$

Taking $\langle T^* \rangle$ = 450 K, as found for the heme group of cytochrome *c* under 10-ns pulsed excitation,[30] leads to $T^*_{pulsed} - T^*_{cw} \sim 150$ K (from eq 10 with T_0 replaced by $\langle T^* \rangle$ under pulsed conditions). Table I and eq 10 suggest that T^*_{cw} does not greatly exceed 300 K for 420-nm excitation ($\Delta E \sim h\nu \sim 4.5 \times 10^{-19}$ J at 420 nm), so that eq 18 and the ratio of pulsed to cw photoreduction cross-sections leads to $E_A \sim 8.3$ kcal/mol for metMb and $E_A \sim 9.5$ kcal/mol for cytochrome *c*. These values are the same magnitude as those obtained using the transient vibrational heating model to fit the cw wavelength dependence of the photoreduction cross-section (Table I).

V. Summary

A variety of heme proteins and their model compounds have been photoreduced under controlled conditions, and the wavelength dependence of the photoreduction and photooxidation cross-sections has been measured quantitatively for the first time. The results demonstrate an exponential increase of the cross-section as the wavelength is decreased from 400 to 250 nm. This type of behavior is not consistent with traditional models that assume excited-state electron transfer is coupled to the major optical transitions of the heme or to the near ultraviolet transitions of the aromatic amino acids.

In order to compare the structures of the photoreduced and chemically reduced species, resonance Raman and absorption spectroscopies were utilized. These studies demonstrate that the heme group, its ligands, and its immediate surroundings are basically unaltered for cytochrome *c*. Small differences are noted between the photoreduced and chemically reduced samples of Mb, which suggest a minor alteration of the distal pocket structure in this system, but no gross protein structural changes are evident. Finally, we find that the photoreduction and photooxidation processes are reversible, and that they can be controlled by choice of excitation wavelength. The fact that significant photoreduction can be carried out with a single 10-ns laser pulse also suggests that heme photoreduction might be useful as a practical method for triggering redox mediated reactions such as the activation of O_2 by cytochrome P450 or the binding of diatomic ligands to conformationally relaxed states of Mb and Hb.

Studies of heme model complexes such as Met-H8PT confirm the view that the aromatic amino acids are not the primary electron donors, since no aromatic residues are present in the model system. The H8PT studies also suggest that solvent access and axial ligand identity play an important role in determining the balance between photoreduction and photooxidation in heme systems.

Further studies in glycerol solvent mixtures, in the presence and absence of oxygen, demonstrate that oxygen greatly enhances the photooxidation rate but has little effect on the photoreduction rate. The role of glycerol (and other alcohols) is not completely resolved, but the present studies indicate that glycerol enhances photoreduction rates and retards photooxidation rates.

Two alternative models for the excited state transport have been developed. The effects of transient vibrational heating of

(55) Morikis, D.; Li, P.; Bangcharoenpaurpong, O.; Sage, J. T.; Champion, P. M. *J. Phys. Chem.* **1991**, *95*, 3391.

the donor–acceptor vibrational subspace are seen to lead naturally to the observed wavelength dependence of the photoreduction cross-section. The parameters derived from the model suggest that a weakly absorbing "doorway" transition, far removed from the excitation wavelengths, could lead to a vibrationally hot transient complex that becomes much more reactive (i.e., hotter) than the thermalized ground state as the wavelength is tuned to the blue. The excited state Arrhenius barrier for such a complex is estimated to be 7–10 kcal/mol using fits to the wavelength dependence of the cw cross-section. Similar values for the barrier height are found when the photoreduction rates in a single 10-ns pulse (where the heme is heated to a photostationary temperature of ~450 K) are compared to the cw rates at 420 nm.

The alternative (and more traditional) model carries its wavelength dependence directly in the absorption cross-section of the "doorway" optical transition. The excited-state transfer rate is dependent on the equilibrium temperature and has no inherent wavelength dependence. We find that a Gaussian (but not a Lorentzian) optical line shape is compatible with the data, so long as the center frequency is fixed near 250 nm (±10 nm) for Mb or 260 nm (±10 nm) for cytochrome *c*. In contrast to the transient heating model, the traditional model predicts a steep fall-off in photoreduction cross-section as the excitation is tuned deeper into the ultraviolet. The two models also differ significantly in their predicted dependence on ambient temperature. The traditional model predicts the usual Arrhenius dependence with respect to T_0, while the transient heating model predicts a rate that is largely independent of ambient temperature so long as T_0 can be neglected compared to $(h\nu - \Delta E)/C_v$.

Additional experiments will be needed to definitely discriminate between the two models. Preliminary measurements of the photoreduction rate of cytochrome *c* as a function of temperature have been carried out using the ν_4 Raman modes of the heme as population standards to monitor the time dependent development of the reduced species under 420-nm cw radiation. We find very weak temperature dependence in k_R, except for a steep rise near 180 K. This not only suggests that transient heating may be important but also indicates that protein structural fluctuations play a significant role in the process. In analyzing such experiments, we must keep in mind the possibility that frequency and temperature dependence in both σ_d^+ and k_E^+ can potentially affect the results. Further studies of the temperature dependence of the photoreduction cross-section will be reported elsewhere.

Overall these studies suggest that photoreduction in heme systems is a reproducible and potentially fundamental reaction. The enhanced cross-section in the ultraviolet suggests a natural method for energy conversion, which may be relevant in the evolution of photoactive chromophores or as a protective mechanism for trapping free radicals. It is interesting to note that the inhibition of photosynthetic electron transport by ultraviolet radiation shows an exponential wavelength dependence[56] that is very similar to the results shown in Figure 7.

Acknowledgment. This work is supported by grants from the NIH AM35090 and NSF 90-16860. We thank the laboratory of Prof. S. G. Sligar (U. of Illinois) for supplying us with samples of cytochrome P450 and b_5.

(56) Cullen, J. J.; Neale, P.; Lesser, M. *Science* **1992**, *258*, 646.
(57) Mahler, H. R.; Cordes, E. H. *Biological Chemistry*; Harper & Row, Publishers: New York and London, 1966; p 207.
(58) Rodgers, K. K.; Sligar, S. G. *J. Am. Chem. Soc.* **1991**, *113*, 9419–9421.
(59) Gunsalus, I. C.; Meeks, J.; Lipscomb, J.; Debrunner, P. *Molecular Mechanisms of Oxygen Activation*; Hayishi, O., Ed.; Academic Press: New York, 1974; p 585.

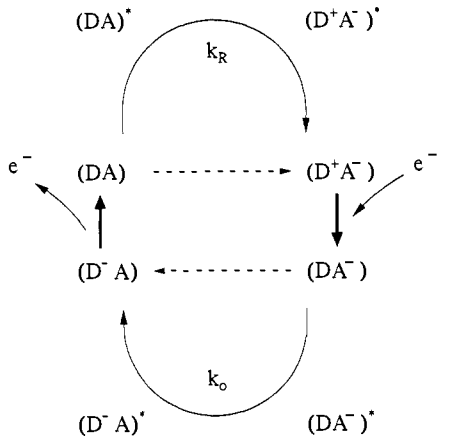

Figure 14. Sketch of the "charge flow" model. Photoreduction and photooxidation processes are indicated by k_R and k_0, respectively. The thick arrows denote rapid decay to more stable states involving the gain or loss of net charge. The photooxidation channel depicted in Figure 1 is effectively blocked by the rapid decay to (DA^-) and replaced by the lower channel shown above. The effective rate equations for k_0 given in Section II are not altered, so long as it is understood that the rates k_L^-, k_E^-, k_b^- refer to the transitions between the corresponding states in the lower channel of the present figure. The dashed lines depict the possibility of ground-state charge transfer within the charge flow model (k_g^* in Figure 1). These rates are negligible in the present application but may play an important role in irreversible biological electron transport processes that take place in the absence of light.

Appendix

Figure 14 depicts a more detailed description of the "charge flow" analysis that is needed to account for the similarity of the photoreduction and photooxidation rates found for the chemically oxidized and reduced protein material. It is important to note that the reactions denoted by the thick solid arrows are much more rapid than the photon-driven rates k_R and k_0. The equilibria are shifted to favor DA and DA^- so that the photoreduction and photooxidation cycles proceed via the different intermediate states, as shown. The expression for the observed photoreduction rate given in Section II still holds, but the underlying fundamental rates need to be reinterpreted for the photooxidation cycle in order to acknowledge that different states are participating in the photooxidation process. Note that in this expanded scheme, D is understood to be the protein (or the local solvent environment), which includes separate donor and acceptor sites for charge transfer to and from the chromophore (A). Thus, in the photooxidation cycle, D actually provides an electron acceptor site for transfer from A^-.

An interesting consequence of this type of model is that it could be very effective in the utilization of photon energy for the irreversible transport of charge. As a simple example, the donor and acceptor sites of D may be located on opposite sides of a membrane. Photons are utilized for moving internal charge in both directions (into and out of A), and the system resets itself. One can imagine the appropriate design (or evolution) of the excited state pairs, so that reduction of A is favored by $(DA)^*$ and $(D^+A^-)^*$ and oxidation of A is favored by $(DA^-)^*$ and $(D^-A)^*$. This would lead to a very efficient coupling of photons (or excitation energy transfer) to a charge transport system.